Theory of coupling in dispersive photonic systems

Bin Xi, Hao Xu, Shiyi Xiao, and Lei Zhou*

State Key Laboratory of Surface Physics and Key Laboratory of Micro and Nano Photonic Structures (Ministry of Education), Fudan University, Shanghai 200433, China

(Received 9 November 2010; revised manuscript received 23 February 2011; published 15 April 2011)

Based on a recently developed Hamiltonian form of Maxwell's equations for dispersive media [A. Raman and S. Fan, Phys. Rev. Lett. **104**, 087401 (2010)], we established a general theoretical framework to study the coupling problems in dispersive photonic systems such as plasmonic materials. Our theory can *quantitatively* determine the coupling strengths between two *dispersive* photonic resonators based on *ab initio* full-wave calculations on realistic structures. The theory is validated by comparing with known rigorous results, where the crucial role of *dispersion correction* is identified. As an application, we studied the coupled localized surface plasmons in a double-nanorod system. The obtained results agree well with full-wave simulations in most cases, and are helpful to study the "dark modes" which are difficult to detect from conventional simulations.

DOI: 10.1103/PhysRevB.83.165115 PACS number(s): 78.67.Pt, 78.20.Bh

I. INTRODUCTION

Considerable attention has recently been paid to the electromagnetic (EM) wave propagations in complex photonic structures such as metamaterials[1–3] and plasmonic materials,[4,5] due to interest in both fundamental physics and potential applications. In particular, couplings between localized EM modes in metallic nanostructures were found to play an important role in controlling the EM properties of such media. For example, Valentine *et al.*[1] recently fabricated a three-dimensional (3D) negative-index optical metamaterial by stacking multiple layers of fishnet structures, and showed that the wide band of negative index resulted from the strong *couplings* between adjacent layers. Liu *et al.*[2] constructed a 3D magnetic metamaterial by stacking multilayers of split ring resonators (SRR), and found a broadening of resonance bandwidth caused by the couplings between different layers. Moreover, when the SRR layers were stacked in a spiral way, the resultant EM eigenmode properties became rather intriguing, caused again by the mutual couplings between these layers.[3] In the field of plasmonics, Maier *et al.*[4] utilized the couplings between adjacent metallic nanoparticles to transmit light energy along a chain of subwavelength particles, and Yang *et al.*[5] recently found that the eigenmodes of a coupled double gold nanohexagon exhibit very intriguing dependence on the relative position of these two nanohexagons. All these experiments suggested that couplings are essential to determine the EM properties of these complex systems.

Theoretical approaches gradually appear to study the coupling problems. For example, an equivalent LC-circuit model was employed to study the couplings between adjacent SRRs,[6] and a dyadic Green's function formalism based on multiple-scattering theory was established to study the plasmonic modes in chains of metallic nanospheres.[7] While these approaches were justified in certain systems (SRRs or spheres), they are not general enough to study the coupling issues in *arbitrary* photonic systems. On the other hand, full-wave simulations were frequently employed to study the wave propagations in coupled metallic nanostructures.[3,8,9] Although such full-wave calculations could well reproduce the experimental data, they typically shed little light on understanding the inherent physics behind the coupling phenomena. In particular, quantitative values of coupling strengths can only be obtained by fitting with some simplified models.[3,6]

The tight-binding method (TBM), originally developed to study the electronic properties of condensed matters, has recently been extended to photonic systems.[10–16] While the TBM is considered a suitable approach to study the coupling effects in complex photonic systems, previous TBMs suffer several limitations. Early photonic versions of TBM are basically *empirical* theories, with hopping integrals (coupling strengths) set as adjustable parameters obtained by fitting with full-wave calculations or experimental data.[10–12] Based on different Hamiltonian forms of Maxwell's equations, several new TBM formalisms[13–16] were recently established, which could *directly* calculate the hopping integrals in coupled photonic systems. However, all these theories[13–16] are only applicable to *nondispersive* systems with *frequency-independent* permittivity ε and permeability μ. This is a severe limitation and makes these theories nonapplicable to most plasmonic systems and optical metamaterials,[1–5] where the constituted materials inevitably possess frequency-dependent $\varepsilon(\vec{r})$. The inherent physical reason is that previous Hamiltonian forms of Maxwell's equations were all developed for nondispersive photonic systems[13–16] and were not applicable to highly dispersive systems such as plasmonics and optical metamaterials.[1–5]

In fact, the coupling issues in *dispersive* photonic systems are much more general and fascinating than those in nondispersive photonic systems (e.g., photonic crystals). For example, while the EM eigenmode is typically the Fabry-Pérot (FP) cavity mode in nondispersive photonic systems,[13–16] in dispersive plasmonic systems, the eigenmode can also be the surface-plasmon (SP) resonance mode,[1–5] in addition to the usual FP one. Therefore, it is highly desirable to set up a *unified* theory to study the coupling issues in *general* photonic systems, no matter if the system is dispersive or not.

Very recently, Raman and Fan established a new Hamiltonian form for Maxwell's equations.[17] An important improvement is that the new Hamiltonian form is applicable to dispersive photonic systems, with frequency dependence in $\varepsilon(\vec{r})$ eliminated by introducing appropriate auxiliary fields.[17] In this paper, based on this new Hamiltonian, we propose a generalized TBM (GTBM) to study the coupling issues

in dispersive photonic systems, particularly in plasmonic materials and optical metamaterials, The GTBM has overcome all the limitations of previous TBMs,[10–16] since it can be applied to *quantitatively* evaluate the coupling strengths in arbitrary photonic systems with dispersive $\varepsilon(\vec{r})$. The theory is justified by comparing with known rigorous results on a model plasmonic system, and the *dispersion correction* is found to play a crucial role in accurately predicting the coupling strengths in plasmonic systems.

This paper is organized as follows. After establishing the theoretical framework of the GTBM in Sec. II, we present some benchmark studies to demonstrate the validity of our theory in Sec. III. The role of dispersion correction is then explicitly discussed in Sec. IV. We next employ the GTBM to examine the general behaviors of the coupled localized surface plasmons (LSPs) in metallic double rods in Sec. V, with conclusions fully supported by full-wave numerical simulations. Finally, we conclude the paper in the last section.

II. THEORETICAL FORMALISMS

We first briefly describe the new Hamiltonian form of Maxwell's equations for dispersive media.[17] Here we only consider such a dispersive medium whose permittivity can be described by a Lorentz (for dielectric) or a Drude model (for metal). To understand the origin of the material's frequency dispersion, let us study the equation of motion for an electron with mass m and charge e driven by an external electric field $\vec{E}$,

$$m\frac{d^2\vec{r}}{dt^2} = e\vec{E} - m\omega_e^2\vec{r} - m\Gamma\frac{d\vec{r}}{dt}, \tag{1}$$

where ω_e is the characteristic frequency of the restoring force and Γ is the damping constant. Defining the polarization field $\vec{P} = Ne\vec{r}$ with N being the electron density, we get

$$\frac{d^2\vec{P}}{dt^2} = \omega_p^2\varepsilon_\infty\vec{E} - \omega_e^2\vec{P} - \Gamma\frac{d\vec{P}}{dt}, \tag{2}$$

where $\omega_p = \sqrt{Ne^2/m\varepsilon_\infty}$ is the plasma frequency with ε_∞ being the permittivity of the background medium. Assuming harmonic time dependence $\exp(i\omega t)$ for all fields, and considering the standard definition of the constitutional relation $\vec{P}(\omega) = \varepsilon_\infty\chi(\omega)\vec{E}(\omega), \varepsilon(\omega) = \varepsilon_\infty[1+\chi(\omega)]$, it is easy to derive from Eq. (2) that

$$\varepsilon(\omega) = \varepsilon_\infty\left[1 + \frac{\omega_p^2}{\omega_e^2 - \omega^2 + i\omega\Gamma}\right], \tag{3}$$

which is the standard Lorentz form of permittivity. It is straightforward to verify that the Drude model is a special case of the Lorentz model by applying $\omega_e = 0$ to Eq. (3). In Maxwell's equations for dispersive media, if we eliminate $\vec{P}$ through the constitutional relation, then a frequency-dependent $\varepsilon(\omega)$ will *inevitably* appear in the resultant frequency-domain Maxwell's equations. However, we can retain the field $\vec{P}$ in Maxwell's equations and further introduce an auxiliary field—the polarization current $\vec{V} = d\vec{P}/dt$.[17] Then, Maxwell's equations (in frequency domain) become

$$\begin{aligned}
\omega\vec{H} &= \frac{i}{\mu}\nabla\times\vec{E},\\
\omega\vec{E} &= -\frac{i}{\varepsilon_\infty}\nabla\times\vec{H} + \frac{i}{\varepsilon_\infty}\vec{V},\\
\omega\vec{P} &= -i\vec{V},\\
\omega\vec{V} &= -i\omega_p^2\varepsilon_\infty\vec{E} + i\omega_e^2\vec{P} + i\Gamma\vec{V},
\end{aligned} \tag{4}$$

which can be further rewritten as a Hamiltonian form,

$$\hat{\mathbf{H}}|\psi\rangle = \omega|\psi\rangle, \tag{5}$$

with the wave function defined as $|\psi\rangle = [\vec{H}\ \vec{E}\ \vec{P}\ \vec{V}]^T$ and the Hamiltonian operator defined as

$$\hat{\mathbf{H}} = \begin{pmatrix} 0 & i\mu^{-1}\nabla\times & 0 & 0\\ -i\varepsilon_\infty^{-1}\nabla\times & 0 & 0 & i\varepsilon_\infty^{-1}\\ 0 & 0 & 0 & -i\\ 0 & -i\omega_p^2\varepsilon_\infty & i\omega_e^2 & i\Gamma \end{pmatrix}. \tag{6}$$

Consider the lossless medium (i.e., $\Gamma = 0$) and define the inner product as

$$\begin{aligned}
\langle\psi_1|\psi_2\rangle = \frac{1}{2}\int d\vec{r}\big[&\mu\vec{H}_1^*\cdot\vec{H}_2 + \varepsilon_\infty\vec{E}_1^*\cdot\vec{E}_2\\
&+\omega_e^2\left(\omega_p^2\varepsilon_\infty\right)^{-1}\vec{P}_1^*\cdot\vec{P}_2 + \left(\omega_p^2\varepsilon_\infty\right)^{-1}\vec{V}_1^*\cdot\vec{V}_2\big],
\end{aligned} \tag{7}$$

it is easy to verify that $\hat{\mathbf{H}}$ is a Hermitian operator.[17] This important property enables us to make a direct analogy between Eq. (5) and Schrödinger's equation for electrons. Here, we note that both $\hat{\mathbf{H}}$ and the inner product are frequency independent although we are treating a dispersive medium with a frequency-dependent permittivity as given by Eq. (3).[18] In what follows, we use f and ω to denote the linear and circular frequencies, respectively.

The theoretical development of the GTBM for dispersive photonic systems is analogous to the establishment of the TBM for electronic systems.[19] Without losing generality, we consider a host homogeneous medium described by a permittivity function $\varepsilon_h(\omega)$ and a permeability μ_h, embedded with several identical photonic scatters, each described by a permittivity function $\varepsilon_s(\omega,\vec{r})$ and a permeability μ_s.[18] Mapping the permittivity functions $\varepsilon_s(\omega,\vec{r})$ and $\varepsilon_h(\omega)$ to the standard Lorentz form as shown in Eq. (3), we get three position-dependent functions, $\varepsilon_{\infty,s}(\vec{r})$, $\omega_{e,s}(\vec{r})$, and $\omega_{p,s}(\vec{r})$, for the scatter, and three constants, $\varepsilon_{\infty,h}$, $\omega_{e,h}$, and $\omega_{p,h}$, for the host medium. In the special case when the scatter is formed by a single homogeneous material, $\varepsilon_{\infty,s}(\vec{r})$, $\omega_{e,s}(\vec{r})$, and $\omega_{p,s}(\vec{r})$ take constant values inside the region the scatter occupies. We first study the system containing only one scatter located at the origin. In this case, the Hamiltonian equation is given by

$$[\hat{\mathbf{H}}_h + \hat{\mathbf{V}}_s(\vec{r})]|\Phi\rangle = 2\pi f_0|\Phi\rangle, \tag{8}$$

where $\hat{\mathbf{H}}_h$ is the Hamiltonian to describe the host medium, and $\hat{\mathbf{V}}_s(\vec{r})$ describes the potential contributed by the scatter,

which is

$$\hat{\mathbf{V}}_s(\vec{r}) = \begin{pmatrix} 0 & i\left(\mu_s^{-1} - \mu_h^{-1}\right)\nabla\times & 0 & 0 \\ -i\left[\varepsilon_{\infty,s}^{-1}(\vec{r}) - \varepsilon_{\infty,h}^{-1}\right]\nabla\times & 0 & 0 & i\left[\varepsilon_{\infty,s}^{-1}(\vec{r}) - \varepsilon_{\infty,h}^{-1}\right] \\ 0 & 0 & 0 & 0 \\ 0 & -i\left[\omega_{p,s}^2(\vec{r})\varepsilon_{\infty,s}(\vec{r}) - \omega_{p,h}^2\varepsilon_{\infty,h}\right] & i\left[\omega_{e,s}^2(\vec{r}) - \omega_{e,h}^2\right] & 0 \end{pmatrix}, \tag{9}$$

inside the region the scatter occupies and is *zero* elsewhere. By solving Eq. (8), we can get a series of eigenmodes with wave functions $|\Phi(\vec{r})\rangle = [\vec{H}_0(\vec{r})\ \vec{E}_0(\vec{r})\ \vec{P}_0(\vec{r})\ \vec{V}_0(\vec{r})]^T$ and corresponding eigen- (linear) frequencies f_0. Consider only those localized states trapped by a single scatter. Mathematically, this requires that the wave function $|\Phi(\vec{r})\rangle$ approaches zero as $|\vec{r}| \to \infty$. For simplicity, here we assume that the system only traps one such localized eigenmode, and the extension to multimodes situation is straightforward.

We now consider the system consisting of a collection of identical scatters. The Hamiltonian can be written as

$$\hat{\mathbf{H}} = \hat{\mathbf{H}}_h + \sum_i \hat{\mathbf{V}}_i, \tag{10}$$

where $\hat{\mathbf{V}}_i$ is the potential term contributed by the ith scatter located at a position $\vec{R}_i$ and $\hat{\mathbf{V}}_i = \hat{\mathbf{V}}_s(\vec{r} - \vec{R}_i)$. When the trapped mode is well bounded by a single scatter, we do not need to really solve the entire Hamiltonian (10). Instead, using only the single-scatter information (f_0 and $|\Phi\rangle$), we can calculate the couplings between different scatters, and in turn, understand the EM properties of the entire system.

We notice that photons now follow exactly the same Hamiltonian form as electrons do. Therefore, all the techniques derived based on Schrödinger's equations[19] can be directly applied here to photons. Under the tight-binding approximation, we found that $\hat{\mathbf{H}}$ can be effectively rewritten in a second quantization form,

$$\begin{aligned} \hat{\mathbf{H}} &= 2\pi \sum_i (f_0 + t_{i,i}) a_i^\dagger a_i + 2\pi \sum_{i \neq j} t_{i,j} a_i^\dagger a_j \\ &= 2\pi \sum_{i,j} H_{i,j} a_i^\dagger a_j, \end{aligned} \tag{11}$$

where $a_i^\dagger$ and a_i are the creation and annihilation operators of photons in the trapped state of the ith scatter. Here a factor 2π is purposely introduced for easy comparison with numerical simulations which usually adopt linear frequencies. The hopping parameters (coupling strengths) are defined as

$$\begin{aligned} t_{i,j} &= \frac{1}{2\pi \langle \Phi \mid \Phi \rangle} \langle \varphi_i | \hat{\mathbf{H}} - (\hat{\mathbf{H}}_h + \hat{\mathbf{V}}_j) | \varphi_j \rangle \\ &= \frac{1}{2\pi \langle \Phi \mid \Phi \rangle} \langle \varphi_i | \sum_{l \neq j} \hat{\mathbf{V}}_l | \varphi_j \rangle, \end{aligned} \tag{12}$$

where $|\varphi_i\rangle = |\Phi(\vec{r} - \vec{R}_i)\rangle$, which is typically termed as the Wannier function in TBM, represents the localized state bounded by the ith scatter. Diagonalizing the Hamiltonian matrix

$$\mathbf{H}_{i,j} = (f_0 + t_{i,i})\delta_{i,j} + t_{i,j}(1 - \delta_{i,j}) \tag{13}$$

enables us to calculate the eigenfrequencies and wave functions of the whole coupled system. Here the language of second quantization[19] is adopted in order to make the presentations concise. However, the same results can be derived without using this language (see the Appendix).

It is intuitive to derive explicit forms for the hopping parameters $t_{i,j}$, in particular, the nearest-neighbor term $t_{1,2}$, which directly measures the *coupling strength* between two neighboring localized states. Since the auxiliary fields $\vec{P}$ and $\vec{V}$ must be zero in the host medium, according to Eq. (12), we get explicitly

$$t_{1,2} \approx \langle \varphi_1 | \hat{\mathbf{V}}_1 | \varphi_2 \rangle = t_{1,2}^H + t_{1,2}^E + t_{1,2}^{\text{disp}} \tag{14}$$

with

$$\begin{aligned} t_{1,2}^H &= \frac{f_0}{2\langle \Phi \mid \Phi \rangle} \int_{S1} d\vec{r} \left[(\mu_h - \mu_s) \right. \\ &\quad \left. \times \vec{H}_0^*(\vec{r} - \vec{R}_1) \cdot \vec{H}_0(\vec{r} - \vec{R}_2) \right], \\ t_{1,2}^E &= \frac{f_0}{2\langle \Phi \mid \Phi \rangle} \int_{S1} d\vec{r} \left[(\varepsilon_{\infty,h} - \varepsilon_{\infty,s}(\vec{r})) \right. \\ &\quad \left. \times \vec{E}_0^*(\vec{r} - \vec{R}_1) \cdot \vec{E}_0(\vec{r} - \vec{R}_2) \right], \\ t_{1,2}^{\text{disp}} &= \frac{f_0}{2\langle \Phi \mid \Phi \rangle} \int_{S1} d\vec{r} \left[\left(-\frac{\omega_{p,s}^2(\vec{r})\varepsilon_{\infty,s}(\vec{r})}{\omega_{e,s}^2(\vec{r}) - (2\pi f_0)^2} \right) \right. \\ &\quad \left. \times \vec{E}_0^*(\vec{r} - \vec{R}_1) \cdot \vec{E}_0(\vec{r} - \vec{R}_2) \right], \end{aligned} \tag{15}$$

where $S1$ defines the region occupied by the scatter 1. Other hopping parameters $t_{i,j}$ including the on-site term $t_{1,1}$, take similar forms as Eqs. (14) and (15), and are easy to derive. However, it is easily expected that those terms are much smaller than $t_{1,2}$, since the trapped mode wave function decays fast to zero when leaving the scatter.

Equations (14) and (15) are the key results that we derived. First, we emphasize again that the coupling strength can be readily calculated once the single-scatter mode information (f_0, $\vec{E}_0$, $\vec{H}_0$, $\vec{P}_0$, $\vec{V}_0$) is available, without necessarily performing the complicated calculations for the whole system. Second, each term in Eq. (14) has very clear physical meaning—$t_{1,2}^H$ denotes the magnetic contribution, $t_{1,2}^E$ is the *nondispersive* electric contribution, and $t_{1,2}^{\text{disp}}$ gives the contribution from the material dispersion. Third, the coupling effect results essentially from the EM interactions *inside* one scatter, represented as the overlapping between wave functions for two neighboring sites. Therefore, the coupling strength depends sensitively on the material properties of the medium forming the scatter.

It is worth mentioning that the presently derived GTBM is general enough to study both dispersive and nondispersive media. In the latter case, we simply set $\omega_{p,s}(\vec{r}) = \omega_{p,h} = 0$ and replace $\varepsilon_{\infty,s}(\vec{r})$, $\varepsilon_{\infty,h}$ by $\varepsilon_s(\vec{r})$, ε_h, which are the permittivity of the scatter and the host medium, respectively. In doing so, the Hamiltonian formalism (6) goes back to that derived by Xu *et al.* for the nondispersive photonic medium,[20] and the GTBM recovers the previously established nondispersive TBM (ND-TBM).[16] In order to make explicit comparisons between the GTBM and ND-TBM, we summarize the key equations in ND-TBM[16] in the following:

$$\langle \psi_1 \mid \psi_2 \rangle = \frac{1}{2} \int d\vec{r} [\mu(\vec{r}) \vec{H}_1^*(\vec{r}) \cdot \vec{H}_2(\vec{r}) + \varepsilon(\vec{r}) \vec{E}_1^*(\vec{r}) \cdot \vec{E}_2(\vec{r})], \tag{16}$$

$$t_{1,2} = \frac{f_0}{2\langle \Phi \mid \Phi \rangle} \int_{S1} d\vec{r} \{[\mu_h - \mu_s(\vec{r})] \vec{H}_0^*(\vec{r} - \vec{R}_1) \cdot \vec{H}_0(\vec{r} - \vec{R}_2) + [\varepsilon_h - \varepsilon_s(\vec{r})] \vec{E}_0^*(\vec{r} - \vec{R}_1) \cdot \vec{E}_0(\vec{r} - \vec{R}_2)\}, \tag{17}$$

which are the definitions of the inner product and the explicit expression for the coupling parameters in nondispersive systems. Here, $\varepsilon(\vec{r})$ and $\mu(\vec{r})$ describe the (nondispersive) permittivity and permeability distributions of the system, f_0 and $|\Phi\rangle = [\vec{E}_0, \vec{H}_0]^T$ denotes the frequency and wave function of a localized eigenmode trapped by a single scatter in nondispersive photonic systems.

III. BENCHMARK STUDIES ON COUPLED SURFACE PLASMON POLARITONS

To validate the presently derived GTBM, we apply it to study the coupled surface-plasmon polaritons (SPPs) in a double-plate system as a benchmark test. Consider a pair of 10-nm-thick gold slabs, placed at the xy plane separated by a distance d. The model parameters for gold are $\mu_s = \mu_0$, $\varepsilon_{\infty,s} = 9\varepsilon_0$, $\omega_{p,s} = [2\pi(\varepsilon_{\infty,s}/\varepsilon_0)^{-1/2}] * 2176.2$ THz, and $\omega_{e,s} = 0$ THz. For simplicity, we neglect the loss by setting $\Gamma = 0$ everywhere.

Consider first the trapped modes in one plasmonic gold slab. With parallel wave vector k_x fixed as a value larger than ω/c (c is the light speed), EM eigenmodes can be found in the system, which are just the SPPs trapped by the slab. To obtain the physical properties of these modes (i.e., f_0, $|\Phi\rangle$), we employ the standard transfer-matrix method (TMM) to study the transmission spectrum of the plasmonic slab under evanescent wave excitations with a fixed k_x, and identify the SPP mode from the divergence in the transmission spectrum. As an illustration, Fig. 1 shows the calculated transmission spectrum of the slab where $k_x = 6.283 \times 10^7$ m^{-1}, from which an eigenmode is easily identified at $f_0 =$ 618.6 THz. It is easy to confirm that at this frequency $\omega/c = 1.295 \times 10^7$ m$^{-1} < k_x$, indicating that such a mode is indeed a SPP. The inset to Fig. 1 depicts the distribution of the field H_y along the z direction for this mode, which confirms that such a mode is an antisymmetrical SPP trapped by the slab.[21] Other field components can be easily derived and are not shown here.

With the physical properties of the single-slab trapped mode known, we then employed the GTBM to compute the hopping parameters in a coupled system consisting of two identical

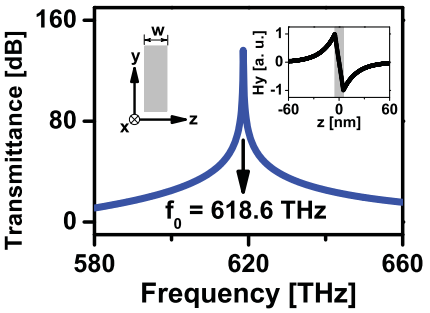

FIG. 1. (Color online) Transmission spectrum through a 10-nm-thick plasmonic slab, calculated by the TMM for the p-polarized incident wave with a fixed $\vec{k}_{||}$ ($k_y = 0, k_x = 6.283 \times 10^7$ m^{-1}). The configuration of the system is shown in the top-left inset. The top-right inset shows the TMM-calculated distribution of H_y along the z axis at the frequency 618.6 THz.

slabs. Setting the interslab distance $d = 40$ nm, we performed numerical calculations based on Eqs. (12) and (15) to find the hopping parameters as $t_{1,2} = t_{2,1} = 13.3$ THz and $t_{1,1} = t_{2,2} = -2.7$ THz. Therefore, the eigenmodes of the coupled system can be obtained by solving the Hamiltonian (11), which is equivalent to diagonalizing the following Hamiltonian matrix:

$$\mathbf{H} = 2\pi \begin{pmatrix} f_0 + t_{1,1}/2 & t_{1,2} \\ t_{2,1} & f_0 + t_{2,2}/2 \end{pmatrix}. \tag{18}$$

Solving the matrix problem (18), we obtain the following two modes:

$$f_+ = f_0 + t_{1,1}/2 + t_{1,2} = 629.2 \text{ THz}, \quad |f_+\rangle = |\varphi_1\rangle + |\varphi_2\rangle, \tag{19}$$
$$f_- = f_0 + t_{1,1}/2 - t_{1,2} = 602.6 \text{ THz}, \quad |f_-\rangle = |\varphi_1\rangle - |\varphi_2\rangle,$$

where $|f_\pm\rangle$ represents the wave functions of the two modes.

To test the accuracy of the GTBM results, we employed the TMM to rigorously calculate the coupled SPP modes in the double-slab system. Figure 2(a) presents the TMM-calculated transmission spectrum through the double-slab system setting again $k_x = 6.283 \times 10^7$ m^{-1}. Two eigenmodes are clearly identified at frequencies 603.2 and 630.2 THz, in excellent agreement with the GTBM results labeled by two vertical lines based on Eq. (19). From the H_y-field distributions presented in Figs. 2(b) and 2(c), we found that the wave functions of the two modes are also in perfect agreement with the GTBM predictions [see Eq. (19)].

We then calculated the frequencies of the coupled SPP modes for different k_x values in the double-slab system. The computed SPP mode frequencies are shown in Fig. 3 as functions of k_x, which agree very well with the dispersion relations calculated with the rigorous TMM. The agreement is found to be better for the larger k_x case where the SPP is more localized around each plasmonic slab so that the tight-binding approximation is better applicable. In smaller k_x cases, slight deviations exist between the GTBM and TMM results, since the SPPs are not tightly bounded by each plasmonic slab. These benchmark tests have unambiguously validated the presently derived GTBM.

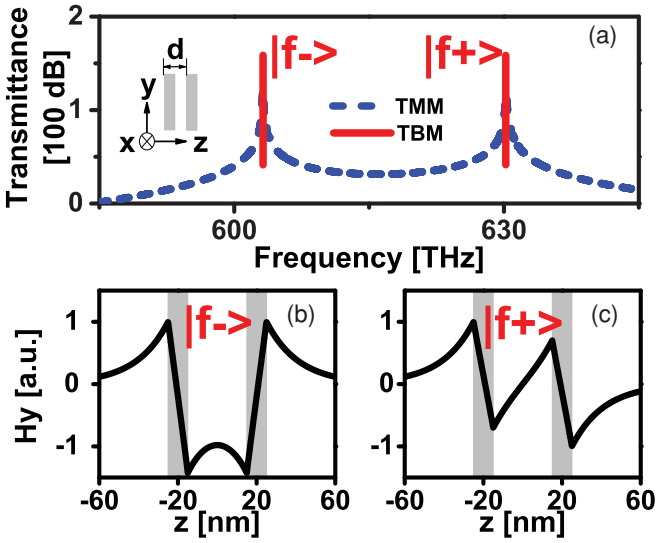

FIG. 2. (Color online) (a) Transmission spectrum through two 10-nm-thick plasmonic slabs separated by 40 nm, calculated by the TMM for the p-polarized incident wave with a fixed $\vec{k}_{||}$ ($k_y = 0, k_x = 6.283 \times 10^7$ m^{-1}). The configuration of the system is shown in the inset. Vertical solid lines denote the positions of the two modes $|f_+\rangle, |f_-\rangle$ predicted by the GTBM. Distributions of H_y along the z axis calculated with the TMM at the frequencies (b) 603.2 THz (the $|f_-\rangle$ mode) and (c) 630.2 THz (the $|f_+\rangle$ mode).

IV. DISPERSION CORRECTION

As we mentioned before, one important advantage of our GTBM is that it can be applied to study the coupling effects in dispersive photonic systems, as already demonstrated in Figs. 2 and 3. In this section, we present a detailed examination of the dispersion correction in the GTBM. In particular, we will discuss in what systems such corrections are important and in what systems the previous ND-TBM[16] is still applicable.

In literature, when considering a dispersive medium with frequency-dependent $\varepsilon(\omega)$, people frequently just assume $\varepsilon = \varepsilon(\omega_0)$ around some frequency (ω_0) of interest, and neglect the additional frequency dependence in $\varepsilon(\omega)$ as ω differs from ω_0. It was usually argued that such an approximation is valid when ω is near ω_0 and when the material dispersion is not strong.

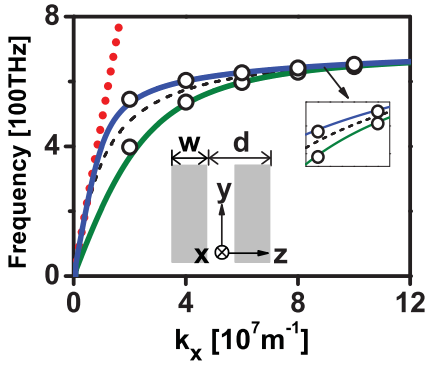

FIG. 3. (Color online) Frequencies (circles) of the coupled SPP modes in the double-plate system, calculated by the GTBM for five different values of k_x ($k_y = 0$). SPP dispersion curves for the double-plate system (solid lines) and the single slab (dashed line), calculated by the TMM. The dotted line represents the light line in air. The inset shows a zoomed view of the dispersion curves.

With the GTBM developed here, we can test the validity of such a treatment.

With the help of Eq. (3), the coupling strength $t_{1,2}$ defined in Eqs. (14) and (15) in the GTBM is rewritten as

$$t_{1,2}|_{\mathrm{GTBM}} = \frac{f_0}{2\langle\Phi \mid \Phi\rangle_{\mathrm{GTBM}}} \times \int_{S1} d\vec{r}[(\mu_h - \mu_s)\vec{H}_0^*(\vec{r} - \vec{R}_1) \cdot \vec{H}_0(\vec{r} - \vec{R}_2) + (\varepsilon_h - \varepsilon_s(\omega_0))\vec{E}_0^*(\vec{r} - \vec{R}_1) \cdot \vec{E}_0(\vec{r} - \vec{R}_2)], \tag{20}$$

where $\langle\Phi \mid \Phi\rangle_{\mathrm{GTBM}}$ is calculated based on Eq. (7).

On the other hand, in ND-TBM, applying $\varepsilon = \varepsilon(\omega_0)$ to Eq. (17), we found that the hopping integral is explicitly written as

$$t_{1,2}|_{\mathrm{ND-TBM}} = \frac{f_0}{2\langle\Phi \mid \Phi\rangle_{\mathrm{ND-TBM}}} \times \int_{S1} d\vec{r}\{(\mu_h - \mu_s)\vec{H}_0^*(\vec{r} - \vec{R}_1) \cdot \vec{H}_0(\vec{r} - \vec{R}_2) + [\varepsilon_h - \varepsilon_s(\omega_0)]\vec{E}_0^*(\vec{r} - \vec{R}_1) \cdot \vec{E}_0(\vec{r} - \vec{R}_2)\}, \tag{21}$$

where $\langle\Phi \mid \Phi\rangle_{\mathrm{ND-TBM}}$ is defined by Eq. (16). Comparing Eqs. (20) and (21), we found that an important difference between the two expressions is the normalization factor $\langle\Phi \mid \Phi\rangle$, which takes different values in different theories. This suggests that the usual procedure $\varepsilon = \varepsilon(\omega_0)$ has indeed taken some "dispersion corrections" into account, at least yielding the correct form of $\int_{S1} d\vec{r}\{[\varepsilon_h - \varepsilon_s(\omega_0)]\vec{E}_0^*(\vec{r} - \vec{R}_1) \cdot \vec{E}_0(\vec{r} - \vec{R}_2)\}$ in the expression of hopping integral [see Eq. (20)].

Let us explore the denominator $\langle\Phi \mid \Phi\rangle_{\mathrm{GTBM}}$ in detail. According to Eq. (7), $\langle\Phi \mid \Phi\rangle_{\mathrm{GTBM}}$ can be separated into two terms corresponding to the integrals inside and outside the scatter. Supposing the host medium is nondispersive, we find that the dispersion correction exists only in the electric part of the integral inside the scatter. Explicitly, we found from Eq. (7) that such an integral in the GTBM is given by

$$\langle\Phi \mid \Phi\rangle_{\mathrm{GTBM}}^{e,in} = \frac{1}{2}\int_{S1} d\vec{r}\left(\varepsilon_\infty + \frac{\omega_p^2\varepsilon_\infty}{\omega_e^2 - \omega_r^2} + \frac{2\omega_0^2\omega_p^2\varepsilon_\infty}{(\omega_e^2 - \omega_r^2)^2}\right) |\vec{E}_0(\vec{r})|^2. \tag{22}$$

It is not difficult to rewrite the above equation as

$$\langle\Phi \mid \Phi\rangle_{\mathrm{GTBM}}^{e,in} = \frac{1}{2}\int_{S1} d\vec{r}\left.\frac{\partial[\omega\varepsilon(\omega)]}{\partial\omega}\right|_{\omega=\omega_0} |\vec{E}_0(\vec{r})|^2. \tag{23}$$

The above equation is quite intuitive, since it just represents the electric energy stored in such a dispersive medium.[22] On the other hand, according to Eq. (16), such a term in the ND-TBM is found as

$$\langle\Phi \mid \Phi\rangle_{\mathrm{ND-TBM}}^{e,in} = \frac{1}{2}\int_{S1} d\vec{r}\left(\varepsilon_\infty + \frac{\omega_p^2\varepsilon_\infty}{\omega_e^2 - \omega_0^2}\right)|\vec{E}_0(\vec{r})|^2 = \frac{1}{2}\int_{S1} d\vec{r}\varepsilon(\omega_0)|\vec{E}_0(\vec{r})|^2. \tag{24}$$

In a nondispersive medium (e.g., $\partial\varepsilon/\partial\omega = 0$), Eqs. (23) and (24) are identical. However, when the medium is dispersive,

there is an important correction term in Eq. (23) due to the dispersion, which is proportional to $\omega_0(\partial\varepsilon(\omega)/\partial\omega)|_{\omega=\omega_0}$. It is worth noting that, while ε can be negative at some particular frequencies, $\partial[\omega\varepsilon(\omega)]/\partial\omega$ is always positive due to the causality requirement.[22] The presence of the dispersion correction is crucial to make the wave-function normalization positive definite, i.e., $\langle\Phi \mid \Phi\rangle > 0$, which is the desired meaningful result. We will see later that such a dispersion correction is very important at frequencies when the dispersion is strong, i.e., $\omega_0(\partial\varepsilon(\omega)/\partial\omega)|_{\omega=\omega_0} >> \varepsilon(\omega_0)$, but can be neglected in the weak-dispersion case. It is worth mentioning that, in most plasmonic and metamaterial systems, the resonance eigenmode is SP-like, requiring a negative ε, and therefore, a proper treatment of dispersion correction is crucial in such systems.[1–5]

To illustrate the importance of the dispersion correction, below we explicitly consider two examples corresponding to the *weak*-dispersion and *strong*-dispersion cases, respectively.

A. Weak-dispersion case

Consider a 40-mm-long metallic waveguide with a 20 mm × 5 mm cross section, inserted with two 1.2-mm-thick dielectric slabs (with $\mu_s = \mu_0$) separated by a distance d. The permittivity of the slab is described by Eq. (3) with $\varepsilon_{\infty,s} = 58.75\varepsilon_0$, $\omega_{p,s} = [2\pi(\varepsilon_{\infty,s}/\varepsilon_0)^{-1/2}] * 6.20$ GHz, and $\omega_{e,s} = 2\pi * 5.08$ GHz. When only a single slab is present in the waveguide, under the TE_{20} mode excitation, TMM calculations reveal that a localized mode is trapped by the dielectric slab inside the waveguide at the frequency $f_0 = 4.46$ GHz. It is easy to identify that such a trapped mode is a FP-like cavity mode. Now consider the coupling between two such localized states when two identical slabs are present inside the waveguide. At the vicinity of f_0, we found that

$$\varepsilon(\omega_0) = 1.11\varepsilon_{\infty,s}, \qquad \omega_0\frac{\partial\varepsilon(\omega)}{\partial\omega}\bigg|_{\omega=\omega_0} = 0.74\varepsilon_{\infty,s}. \quad (25)$$

Although the term $\omega_0[\partial\varepsilon(\omega)/\partial\omega]|_{\omega=\omega_0}$ is not very small compared to $\varepsilon(\omega_0)$, recalling that the dispersion correction only exists inside the scatter, we understand that the effect of dispersion correction will be further reduced, and therefore it should not be very significant in this case. Indeed, we employed both GTBM and ND-TBM to calculate the hopping integrals $(t_{1,2}, t_{11})$ for such systems with different values of d, and depicted the corresponding mode frequency splitting $\delta f = f_+ - f_-$ [calculated based on Eq. (19)] in Fig. 4 as functions of d. As a comparison, we also depicted the rigorous TMM results for δf as functions of d in Fig. 4. While the GTBM results are certainly in better agreement with the rigorous TMM results, the deviations between the ND-TBM and the TMM results are not very significant. In the limit of $d \to \infty$, both theories give the same results, since the splitting is small and the frequency dispersion is less and less important.

B. Strong-dispersion case

We found that the model system discussed in Sec. III is just a strong-dispersion case, for which the dispersion correction is very important. Apparently, the eigenmode in that system is

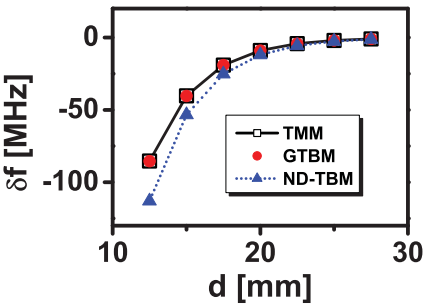

FIG. 4. (Color online) Mode frequency splitting δf as functions of d in the weak-dispersion case, calculated by the TMM (black squares), the GTBM (red circles), and the ND-TBM (blue triangles).

a SP-type resonance mode, which is different from the weak-dispersion case. Taking the material properties given in the last section, at the single-slab SPP frequency $f_0 = 618.6$ THz, we found that

$$\varepsilon(\omega_0) = -0.38\varepsilon_{\infty,s}, \qquad \omega_0\frac{\partial\varepsilon(\omega)}{\partial\omega}\bigg|_{\omega=\omega_0} \approx 2.75\varepsilon_{\infty,s}. \quad (26)$$

The above equation reveals that dispersion correction must be very significant here, since the term $\omega_0[\partial\varepsilon(\omega)/\partial\omega]|_{\omega=\omega_0}$ is not only very large but also exhibits a different sign compared with the term $\varepsilon(\omega_0)$. Therefore, we will have completely different values (with even different signs) as we include or do not include the dispersion correction.

To explicitly illustrate the role of dispersion correction, we again employed both the GTBM and ND-TBM to calculate the frequency splitting δf of the coupled SPP modes in the double-slab systems assuming that $k_x = 6.283 \times 10^7\ \mathrm{m}^{-1}$. The calculated results are depicted in Fig. 5 as functions of d, compared with the rigorous results calculated with the TMM. Comparisons show that the ND-TBM results are over 100 times larger than the rigorous TMM, while the GTBM yields almost the same results with the TMM ones (see the zoomed view in the inset). Such a significant deviation indicates that, in plasmonic systems with strong material dispersion, dispersion correction must be accurately taken into account and the ND-TBM is totally inapplicable to such systems.

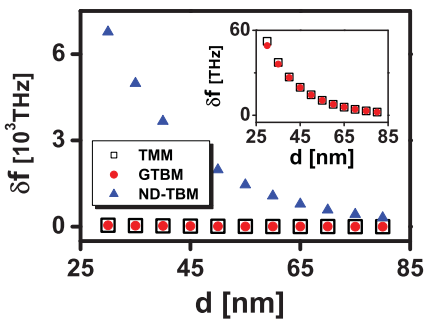

FIG. 5. (Color online) Mode frequency splitting δf as functions of d in the strong-dispersion case, calculated by the TMM (black square), the GTBM (red circles), and the ND-TBM (blue triangles). The inset shows a zoomed view of the results obtained by the TMM and GTBM.

V. APPLICATIONS TO COUPLED LOCALIZED SURFACE PLASMONS

The GTBM developed in this paper can be employed to study the general coupling problems in different photonic systems. We have applied the GTBM to study the coupled SPPs in last two sections, and in this section, we further apply the GTBM to study the couplings between LSPs in nanoplasmonic particles. Different from a SPP in which the field is localized along one direction, the wave function of a LSP is localized around the nanoparticle along all three directions. Rigorous solutions are usually difficult to obtain for such problems (particularly for complex particle shapes). Therefore, the present approach can provide important insights into understanding the inherent physics in such problems.

Consider a system consisting of two identical gold nanorods, each modeled as a finite-length cylinder with both ends capped by hemispheres (Fig. 6). The nanorod has a diameter D fixed at 16 nm, and is characterized by the aspect ratio defined as $R = L/D$ with L being the total length of the rod. The permittivity of gold is described by the Drude model [Eq. (3)] with $\varepsilon_{\infty,s} = 9\varepsilon_0$, $\omega_{p,s} = (2\pi\varepsilon_{\infty,s}^{-1/2}) * 2176.2$ THz, $\omega_{e,s} = 0$ THz, and $\Gamma_s = (2\pi) * 12.09$ THz.[23]

Following the GTBM developed in Sec. II, we first employed the numerical finite elements method (FEM) to get the full information [i.e., f_0 and $\vec{E}_0(\vec{r})$, $\vec{H}_0(\vec{r})$] of a LSP mode trapped by a single gold nanorod.[24] Figure 6 shows the calculated forward transmission spectrum for an individual nanorod (with $R = 3$) illuminated by an incident plane wave with $\vec{E}$ parallel to the rod axis, where a LSP mode is clearly identified at 508.2 THz corresponding to a transmission dip.[25] The nature of this mode can be understood by examining the electric-field distribution at the resonance frequency. The distribution of E_y on the x-y plane depicted in the inset indicates that such a trapped mode is a dipolar plasmon mode polarized along the rod axis. The field information of this mode [i.e., $\vec{E}_0(\vec{r})$ and $\vec{H}_0(\vec{r})$] can be extracted from the numerical calculation results through subtracting the background incident EM field.

We now study the couplings between the LSPs in a pair of identical gold nanorods separated by a distance 36 nm, with geometry shown in the inset to Fig. 7. Following the

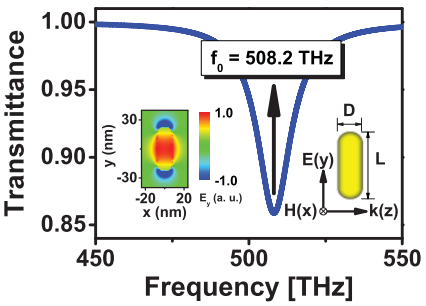

FIG. 6. (Color online) Forward transmission spectrum for an individual gold nanorod ($D = 16$ nm, $L = 48$ nm, see the bottom-right inset), calculated by the FEM with input plane wave polarized such that the E field is parallel to the rod axis. The bottom-left inset depicts the distribution of E_y on the x-y plane, calculated by the FEM at the LSP resonance frequency, 508.2 THz.

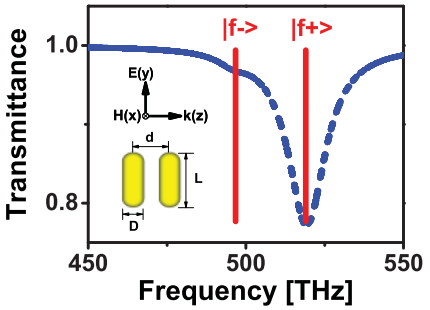

FIG. 7. (Color online) Forward transmission spectra (dashed line) for a coupled gold nanorod pair ($D = 16$ nm, $L = 48$ nm, and $d = 36$ nm), calculated by the FEM with incident plane wave as described in the inset. Vertical solid lines denote the positions of two coupled LSP modes ($|f_+\rangle$, $|f_-\rangle$), calculated by the GTBM.

same procedures as described in Sec. III, we employed the GTBM to calculate the hopping parameters and found that $t_{1,2} = 11.14$ THz and $t_{1,1} = -0.31$ THz. Therefore, the GTBM predicted that the coupled LSP mode frequencies in the double-rod system should be $f_+ = 519.19$ and $f_- = 496.91$THz, according to Eq. (19). To test this prediction, we shined a plane wave with $\vec{E}||\hat{y}$ and $\hat{k}||\hat{z}$ (see Fig. 7) onto the double-rod system, and measured the forward transmission spectrum. Two resonance frequencies appear in the spectrum as shown in Fig. 7, whose positions are in excellent agreement with the GTBM predictions labeled by two vertical solid lines. In addition, the symmetry of the wave functions for the two LSP modes also agree well with the GTBM predictions—the resonance mode at 519.19 THz (496.91 THz) is an in-phase (antiphase) combination of the two LSP modes in different rods.

Now that the GTBM can accurately predict the coupling strength between two plasmonic resonators, we next employ the GTBM to study the general behaviors of the coupling strength (measured by $t_{1,2}$) between neighboring LSPs. In particular, we will study how the coupling strength depends on various factors, including the distance d between two rods and the aspect ratio R of a single rod. With $D = 16$ nm and $R = 3$ fixed, numerical calculations are performed for five values of d and the computed coupling strength is depicted in Fig. 8(a) as a function of d. We note that the hopping parameter $t_{1,2}$ is a decreasing function of d. This is reasonable since the coupling is dictated by the overlapping between the wave-function tails of two LSP modes, and therefore, the larger the separation d, the weaker the coupling strength. Analyzing the numerical data shows that the coupling strength $t_{1,2}$ exhibits a power-law dependence on d, $t_{1,2} \sim d^{-2.05}$. Ideally, in the near-field region, the wave function of a dipolar LSP decays as r^{-3} when leaving the scatter under the quasistatic approximation.[26] Therefore, ideally the hopping parameter should also exhibit a $t_{1,2} \sim d^{-3}$ dependence on d. Here, the discrepancy in the power-law exponent suggests that each single plasmonic resonator cannot be considered as an ideal infinitesimal electric dipole, and the GTBM should be applied to take account of all complicated effects in realistic situations.

Numerical calculations were also performed to study the aspect-ratio R dependence of the coupling strength, and the results are shown in Fig. 8(b) as open circles, where

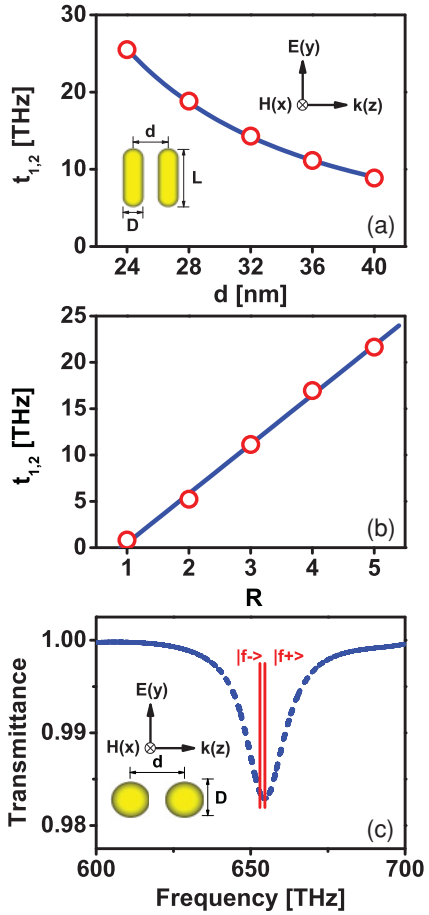

FIG. 8. (Color online) (a) GTBM-calculated coupling strength $t_{1,2}$ between two gold nonorods (circles) as a function of d (with D and L fixed as 16 and 48 nm, see inset for the geometry), with the solid (blue) line representing the fitting curve $t_{1,2} = 17021.72d^{-2.05}$. Propagation and polarization directions of the incident plane wave are depicted in the inset. (b) GTBM-calculated coupling strength $t_{1,2}$ (circles) as a function of the aspect ratio R of the nanorod (with D and d fixed as 16 and 36 nm), with the solid (blue) line representing the fitting curve $t_{1,2} = -4.849 + 5.336R$. (c) FEM calculated transmission spectrum (dashed line) for a coupled gold nanosphere pair ($D = 16$ nm, $d = 36$ nm) under a plane-wave excitation, with $|f+\rangle$ and $|f-\rangle$ denoting the in-phase and antiphase coupled LSP modes, respectively. Frequencies of these two modes calculated by the GTBM are marked by two vertical solid lines.

other parameters are fixed as $D = 16$ nm and $d = 36$ nm. Surprisingly, the coupling strength can still vary dramatically with respect to R, even with a fixed particle separation d. This strong dependence must come from the near-field coupling effect between two plasmonic nanoparticles. Such a dependence can be well fitted by a linear function $t_{1,2} \sim R$, as shown in Fig. 8(b). In particular, in the case of $R = 1$ which corresponds to a nanosphere case, the splitting of two coupled LSP modes is very small according to the GTBM [see Fig. 8(b)]. In fact, these two modes cannot be clearly distinguished from the transmission spectrum excited by a plane wave, as shown in Fig. 8(c). This is the well-known *dark-mode* problem faced by many full-wave simulation techniques, with the physical reason being that the antiphase mode exhibits a very weak radiation strength (also called a dark mode) and thus being buried by the nearby strong in-phase bright mode.[27] However, we note that the GTBM can accurately predict the resonance frequencies of both bright and dark modes [see vertical lines in Fig. 8(c)], independent of their individual radiation strengths. Therefore, for those photonic systems possessing the dark-mode problems, the GTBM established here provides an independent way to accurately identify the eigenmode frequencies of the system, no matter how weakly such modes couple to incident far-field excitations.

VI. CONCLUSIONS

In this paper, we established a generalized tight-binding method to study the coupling effects in dispersive photonic structures. The coupling strength and the resonance frequencies in coupled plasmonic systems can be computed from full-wave numerical calculations without any fitting procedures, and the dispersion correction contributed by the material's frequency dispersion is found to play a crucial role in obtaining correct results. As a benchmark test, we applied the theory to study the coupled SPPs in plasmonic double slabs, and found the obtained results are in perfect agreement with known rigorous solutions. The theory was employed to study the general behaviors of the coupling effects in double nanorods. The obtained results are in excellent agreement with full-wave simulations in most cases, and the GTBM is found of particular importance in identifying those dark modes which are weakly coupled to incident excitation fields. Finally, we note that the GTBM established in this paper is very general and it can be applied to study many other coupling-related problems in complex metamaterials such as the coupled SRRs[28–31] and chiral structures.[32,33]

ACKNOWLEDGMENTS

This work was supported by National Natural Science Foundation of China (No. 60725417 and No. 60990321), Shanghai Science and Technology Committee (08dj1400302), and Ministry of Education of China (B06011).

APPENDIX: DERIVATION OF EQ. (11) IN A MATRIX FORM

In this Appendix, we adopt a standard matrix technique to derive Eq. (11), which is written as a sophisticated second quantization form. Suppose that Eq. (8) has been solved yielding all information for a localized mode trapped by a single scatter located at the origin, then for the same scatter but located at a point $\vec{R}_i$ with potential $\hat{\mathbf{V}}_i = \hat{\mathbf{V}}(\vec{r} - \vec{R}_i)$, we must have

$$(\hat{\mathbf{H}}_h + \hat{\mathbf{V}}_i)|\varphi_i\rangle = 2\pi f_0 |\varphi_i\rangle, \tag{A1}$$

where $|\varphi_i\rangle = |\Phi(\vec{r} - \vec{R}_i)\rangle$. Now consider the case with N identical scatters situated at points $\{\vec{R}_i\}$; the wave function $|\Psi\rangle$ and eigenfrequency f of the entire system must satisfy the Hamiltonian equation

$$\left(\hat{\mathbf{H}}_h + \sum_i \hat{\mathbf{V}}_i\right)|\Psi\rangle = 2\pi f |\Psi\rangle. \tag{A2}$$

We can expand $|\psi\rangle$ as a linear combination of the localized function $|\varphi_i\rangle$,

$$|\Psi\rangle = \sum_i c_i |\varphi_i\rangle, \tag{A3}$$

where c_i is a set of coefficients to be determined. When the scatters are well separated in space, to a very good approximation, we have the orthogonality relation

$$\langle \varphi_i \mid \varphi_j \rangle = \delta_{ij} \langle \Phi(\vec{r}) \mid \Phi(\vec{r}) \rangle. \tag{A4}$$

Applying Eq. (A3) to Eq. (A2) and multiplying both sides by $\langle \varphi_j |$, we obtain

$$\sum_i \langle \varphi_j | \left(\hat{\mathbf{H}}_h + \hat{\mathbf{V}}_i + \sum_{l \neq i} \hat{\mathbf{V}}_l \right) |\varphi_i\rangle c_i = 2\pi f \sum_i c_i \langle \varphi_j \mid \varphi_i \rangle. \tag{A5}$$

Applying Eqs. (A1) and (A4) to Eq. (A5) , we obtain finally

$$\sum_i [\mathbf{H}_{j,i} - f \cdot \delta_{ji}] c_i = 0, \tag{A6}$$

where

$$\mathbf{H}_{j,i} = (f_0 + t_{i,i})\delta_{j,i} + t_{j,i}(1 - \delta_{j,i}) \tag{A7}$$

with $t_{j,i}$ defined as

$$t_{j,i} = \frac{\langle \varphi_j | \sum_{l \neq i} \hat{\mathbf{V}}_l |\varphi_i\rangle}{2\pi \langle \Phi \mid \Phi \rangle}. \tag{A8}$$

Equations (A6) and (A7) are just the matrix representations of Eq. (11), and Eq. (A8) is the same as Eq. (12).

*phzhou@fudan.edu.cn

[1] J. Valentine, S. Zhang, T. Zentgraf, E. Ulin-Avila, D. A. Genov, G. Bartal, and X. Zhang, Nature (London) **455**, 376 (2008).

[2] N. Liu, H. Guo, L. Fu, S. Kaiser, H. Schweizer, and H. Giessen, Nat. Mater. **7**, 31 (2008).

[3] N. Liu, H. Liu, S. Zhu, and H. Giessen, Nat. Photonics **3**, 157 (2009).

[4] S. A. Maier, P. G. Kik, H. A. Atwater, S. Meltzer, E. Harel, B. E. Koel, and A. A. G. Requicha, Nat. Mater. **2**, 229 (2003).

[5] S.-C. Yang, H. Kobori, C.-L. He, M.-H. Lin, H.-Y. Chen, C. Li, M. Kanehara, T. Teranishi, and S. Gwo, Nano Lett. **10**, 632 (2010).

[6] H. Liu, D. A. Genov, D. M. Wu, Y. M. Liu, Z. W. Liu, C. Sun, S. N. Zhu, and X. Zhang, Phys. Rev. B **76**, 073101 (2007).

[7] K. H. Fung and C. T. Chan, Opt. Lett. **32**, 937 (2007).

[8] J. Zhou, T. Koschny, M. Kafesaki, and C. M. Soukoulis, Phys. Rev. B **80**, 035109 (2009).

[9] H. Xu, Z. Wang, J. Hao, J. Dai, L. Ran, J. A. Kong, and L. Zhou, Appl. Phys. Lett. **92**, 041122 (2008).

[10] E. Lidorikis, M. M. Sigalas, E. N. Economou, and C. M. Soukoulis, Phys. Rev. Lett. **81**, 1405 (1998).

[11] Y. Hara, T. Mukaiyama, K. Takeda, and M. Kuwata-Gonokami, Phys. Rev. Lett. **94**, 203905 (2005).

[12] M. Notomi, E. Kuramochi, and T. Tanabe, Nat. Photonics **2**, 741 (2008).

[13] A. Yariv, Y. Xu, R. K. Lee, and A. Scherer, Opt. Lett. **24**, 711 (1999).

[14] K. Busch, S. F. Mingaleev, A. Garcia-Martin, M. Schillinger, and D. Hermann, J. Phys.: Condens. Matter **15**, R1233 (2003).

[15] D. Leuenberger, R. Ferrini, and R. Houdre, J. Appl. Phys. **95**, 806 (2004).

[16] H. Xu, Q. He, S. Xiao, B. Xi, J. Hao, and L. Zhou, J. Appl. Phys. **109**, 023103 (2011).

[17] A. Raman and S. Fan, Phys. Rev. Lett. **104**, 087401 (2010).

[18] For simplicity, we only consider the frequency dispersion in permittivity and assume the permeability of the system as frequency independent. Extensions to the permeability-dispersion case can be done similarly.

[19] N. F. Mott and H. Jones, *The Theory of the Properties of Metals and Alloys* (Oxford University Press, Oxford, 1936).

[20] Y. Xu, Y. Li, R. K. Lee, and A. Yariv, Phys. Rev. E **62**, 7389 (2000).

[21] Another SPP mode with a symmetrical *H*-field pattern was identified at a higher frequency, and the coupling effects related to this mode were also studied by the GTBM, yielding results in excellent agreement with TMM calculations. For the purpose of better illustration in this paper, we only presented the results related to the antisymmetrical SPP modes (Figs. 1–3) because the coupling strength between such modes is much stronger than that between two symmetrical SPP modes.

[22] L. D. Landau and E. M. Lifshitz, *Quantum Mechanics: Non-Relativistic Theory*, 3rd ed. (Butterworth-Heinemann, Oxford, 1981).

[23] V. Myroshnychenko, J. Rodríguez-Fernandez, I. Pastoriza-Santos, A. M. Funston, C. Novo, P. Mulvaney, L. M. Liz-Marzanb, and F. J. G. d. Abajo, Chem. Soc. Rev. **37**, 1792 (2008).

[24] COMSOL MULTIPHYSICS 3.5, developed by COMSOL © (2008).

[25] It should be noted that, different from Figs. 1 and 2 where a SPP is identified as a transmission peak in the spectrum, here the LSP mode corresponds to a transmission dip in the spectrum. Such a difference is caused by the fact that the excitation wave is evanescent in the SPP case but is a plane wave in the LSP case.

[26] J. D. Jackson, *Classical Electrodynamics*, 3rd ed. (Wiley, New York, 1999).

[27] A. M. Funston, C. Novo, T. J. Davis, and P. Mulvaney, Nano Lett. **9**, 1651 (2009).

[28] N. Liu and H. Giessen, Opt. Express **16**, 21233 (2008).

[29] I. Sersic, M. Frimmer, E. Verhagen, and A. F. Koenderink, Phys. Rev. Lett. **103**, 213902 (2009).

[30] H. Liu, Y. M. Liu, T. Li, S. M. Wang, S. N. Zhu, and X. Zhang, Phys. Status Solidi B **246**, 1397 (2009).

[31] K. Aydin, I. M. Pryce, and H. A. Atwater, Opt. Express **18**, 13407 (2010).

[32] A. Andryieuski, C. Menzel, C. Rockstuhl, R. Malureanu, F. Lederer, and A. Lavrinenko, Phys. Rev. B **82**, 235107 (2010).

[33] Z. Li, H. Caglayan, E. Colak, J. Zhou, C. M. Soukoulis, and E. Ozbay, Opt. Express **18**, 5375 (2010).